THE JOURNAL OF PHYSICAL CHEMISTRY C

Article

pubs.acs.org/JPCC

Edge Effects on the pH Response of Graphene Nanoribbon Field Effect Transistors

Xuebin Tan,[†] Hsun-Jen Chuang,[‡] Ming-Wei Lin,[‡] Zhixian Zhou,[‡] and Mark Ming-Cheng Cheng*,[†]

[†]Department of Electrical and Computer Engineering, Wayne State University, Detroit, Michigan 48202, United States

[‡]Department of Physics and Astronomy, Wayne State University, Detroit, Michigan 48201, United States

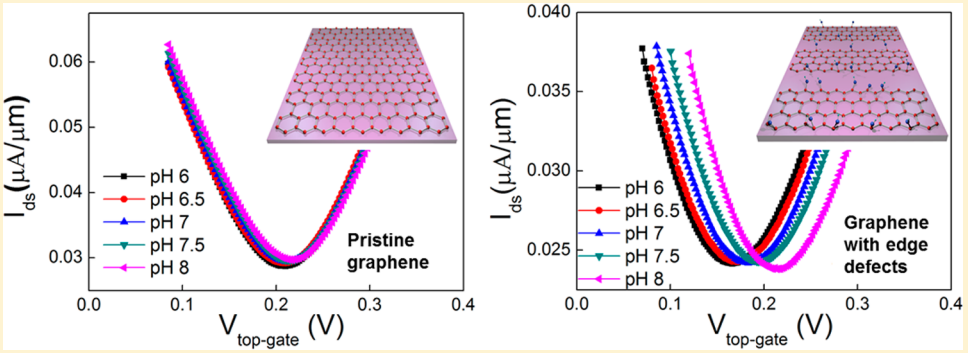

ABSTRACT: We report the pH response enhancement of the electrolyte-gated graphene field effect transistors by controllably introducing edge defects. An average improvement of pH response from 4.2 to 24.6 mV/pH has been observed after downscaling the pristine graphene into graphene nanoribbon arrays with electron beam lithography (EBL) and oxygen plasma. We attribute the improved pH response in graphene nanoribbons to the increased number of hydroxyl groups attached to edge defects as the edge length to surface area ratio increases with decreasing graphene nanoribbon width. Moreover, the shift of the Dirac point in response to the pH change has been found to be reversible, indicating that the hydroxyl ions are binding to the edge defect sites of the graphene nanoribbons through physical adsorption.

INTRODUCTION

Graphene is a single atomic layer of graphite that has extremely high carrier mobility and thermal conductivity[1−4] and is chemically and thermally stable,[5] offering the most tantalizing prospect of high performance carbon-based electronics for the post-silicon era. As the electrons/holes in graphene are confined to an atomically thick plane, the electrical conductance of graphene is extremely sensitive to its surroundings such as substrates,[6] dielectric media,[7] and adsorbed foreign molecules,[8] making graphene an ideal sensing material for label-free chemical and biological sensors. Schedin et al. demonstrated that micrometer-size gas sensors made from graphene were capable of detecting the adsorption and desorption of individual gas molecules.[8] Such high sensitivity was attributed to the unique combination of graphene's two-dimensional (2D) nature (extremely large surface to volume ratio), low noise level due to its relatively high conductivity and few crystal defects, and the possibility of fabricating graphene devices with ohmic electrical contacts.

Graphene has also been studied for pH,[9] chemical, and biological sensor applications.[10] However, a large variation in pH response has been reported for pH sensors based on graphene field effect transistors (FETs), ranging from ∼0 mV/pH to as high as 99 mV/pH.[9,11−15] Fu et al. have recently shown that pristine graphene is insensitive to pH changes in solution and large variation in the pH-induced gate-voltage shift could be attributed to the variation of graphene quality.[11] Similarly, defect-free carbon nanotube (CNT) FETs only respond to the electrostatic potential rather than the pH changes.[16] The insensitivity of graphene and CNT FETs to pH changes could be attributed to the lack of free bonds on the sp^2 bond saturated pristine graphene surface. On the other hand, dangling bonds are anticipated on the surface of defective graphene. Chemical groups such as hydroxyl groups can easily attach to the defect sites of defective graphene through dangling bonds.[17,18] The attached hydroxyl groups can be protonized to OH_2^+ as the pH decreases or deprotonized to O^- as the pH increases. As a result, positively charged OH_2^+ and negatively charged O^- on the graphene surface induce n-type and p-type doping in the graphene channel, respectively. Therefore, in order to improve the sensitivity of the graphene pH sensor, it is necessary to increase the density of the hydroxyl groups attached to the graphene channel.

In contrast to the chemically inert basal plane, the edges of graphene are chemically reactive and can be relatively easily functionalized.[19] For example, graphene nanoribbons (GNR) can be functionalized by nitrogen species at the edges, leading to n-type electronic doping.[20] Moreover, edge doping was

Received: September 11, 2013
Revised: December 4, 2013

   dx.doi.org/10.1021/jp409116r | J. Phys. Chem. C XXXX, XXX, XXX−XXX

shown to be over 3 orders of magnitude more efficient than that induced by adsorbates on the surface.[21] Amin et al. have reported significant sensitivity improvement in graphene-based chemical sensors by cutting the 2D graphene sheets into microribbons with sizes comparable to the line defects.[22] Similar to the defects in the graphene basal plane, edges are also expected to be receptive to the attachment of hydroxyl groups, which is crucial for pH sensing through the protonization and deprotonization processes. Furthermore, the edges of graphene are less disruptive to the current flow in the graphene channel compared to the defects in the basal plane which can seriously degrade the electrical properties of the graphene channel. High mobility values over 3000 $cm^2\ V^{-1}\ s^{-1}$ have been observed in low-disorder GNRs as narrow as 20 nm, suggesting that patterning graphene into GNRs (or arrays of GNRs) is a viable route to creating free bonds for hydroxyl groups to attach to without compromising the excellent electrical characteristics of the graphene sensors.[23]

In this article, we report a systematic study of the effects of defects and edges on the pH response of graphene pH sensors by (1) correlating Raman spectroscopy with pH-induced gate voltage shifts in the transfer characteristics of graphene FETs and (2) patterning 2D graphene sheets into arrays of GNRs to significantly increase the density of attached hydroxyl groups. We observe a slightly increased pH response in graphene devices with a higher level of disorder as quantified by the D-band to G-band intensity ratio in the Raman spectra of the device channel made of chemical vapor deposition (CVD) grown graphene. We further demonstrate, for the first time, that the sensitivity of graphene pH sensors could be controllably increased by patterning the graphene channel into arrays of GNRs with decreasing width, without degrading the electrical properties of the graphene channel. As the width of each GNR in a channel is reduced from 40 μm to 200 nm (or below), the pH response of the devices increases from ~0 to ~25 mV/pH. This significant improvement can be attributed to the increased number of hydroxyl groups attached to the edges per unit area as the edge to surface area ratio increases with decreasing GNR width.

METHODS

Figure 1 shows the process flow for the fabrication of graphene FETs. The pristine graphene used in this study was grown on copper using a chemical vapor deposition (CVD) method.[24,25] Subsequently, graphene was transferred onto a silicon substrate with 300 nm thermal oxide following a method described in the literature.[25] Briefly, the CVD graphene was grown on a 25 μm thick copper foil (Alfa Aesar) in a mixture of methane and hydrogen at 1000 °C. A layer of 200 nm thick poly(methyl methacrylate) (PMMA) was spin-coated and dried at room temperature. After removing the graphene on the backside of the copper using oxygen plasma, the copper foil was etched away using diluted copper etchant (APS-100) for 24 h. The PMMA/graphene film was cleaned using a modified RCA cleaning procedure.[25] PMMA/graphene films were transferred onto the silicon substrate by carefully scooping it out from the solution. Finally, PMMA was dissolved by acetone and left only graphene on top of the substrate as shown in Figure 1a. Graphene channels were defined by a standard photolithography and oxygen plasma etching. Next, the source/drain electrodes were fabricated by depositing 10 nm Ti and 50 nm Au by an electron-beam evaporation system (Temescal BJD 1800) as shown in Figure 1b. In order to controllably create

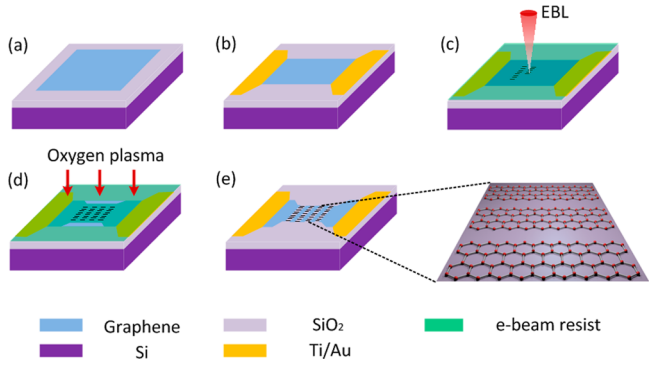

Figure 1. Fabrication process of FET devices made of graphene nanoribbons: (a) transfer of CVD graphene onto SiO_2/Si substrates; (b) graphene patterning and contact metal deposition; (c) graphene nanoribbon patterning with EBL by using PMMA as the e-beam resist; (d) graphene etching by oxygen plasma; (e) GNR array FET after removing the PMMA.

edge defects, GNR arrays of different widths were further fabricated using electron-beam lithography (EBL) as shown in Figure 1c. For EBL, a positive e-beam resist (PMMA) was spin-coated, selectively exposed by e-beam, and developed. Subsequently, oxygen plasma was used to remove the excess graphene to form nanoribbons (Figure 1d). Finally, PMMA was removed by acetone (Figure 1e). HSQ resist was also used to pattern GNRs. After development and oxygen plasma etching to form GNRs, HSQ was removed by buffered oxide etch (BOE) to minimize the doping effects.[21,26] Before testing, the device was annealed at 600 °C with flow of forming gas (H_2/Ar) to remove the resist residue.[27]

To characterize the pH response of the graphene FET devices, a droplet of pH solution was deposited on the device to cover the graphene channel. The transfer characteristics of the device were measured by a silver/silver chloride (Ag/AgCl) reference gate electrode. A semiconductor parameter analyzer (Keithley 4200) was used to measure the drain-source current as a function of the gate voltage by applying a constant low drain-source voltage of 10 mV. The leak current through the gate electrode was also monitored to ensure that it was negligibly small compared to the drain-source current. All the pH solutions ($6 \leq pH \leq 8$) were prepared using phosphate buffered saline (PBS) as a buffer solution with a phosphate concentration of 2−3 mM. The devices were rinsed with an ample amount of deionized water to thoroughly wash away the adsorbates each time before changing to a different pH solution.

RESULTS AND DISCUSSION

Figure 2a shows an optical microscopic image of a representative FET device made of pristine graphene. The graphene was patterned into a dumbbell shape with a dimension of 80 μm by 50 μm. The edge length to surface area ratio in the graphene channel, $S = L/A$, was estimated to be around 0.04 μm^{-1}, where L is the total length of the graphene edge and A is the total area of the graphene channel. Figure 2b schematically illustrates the experiment setup for the pH sensing measurement using the graphene FET in electrolytes with a leakage free solid-state reference electrode (eDAQ ET-072). The electrical double layer at the graphene/electrolyte interface functions as a top gate dielectric of FET. The thickness of the double layer is a function of ionic

dx.doi.org/10.1021/jp409116r | J. Phys. Chem. C XXXX, XXX, XXX−XXX

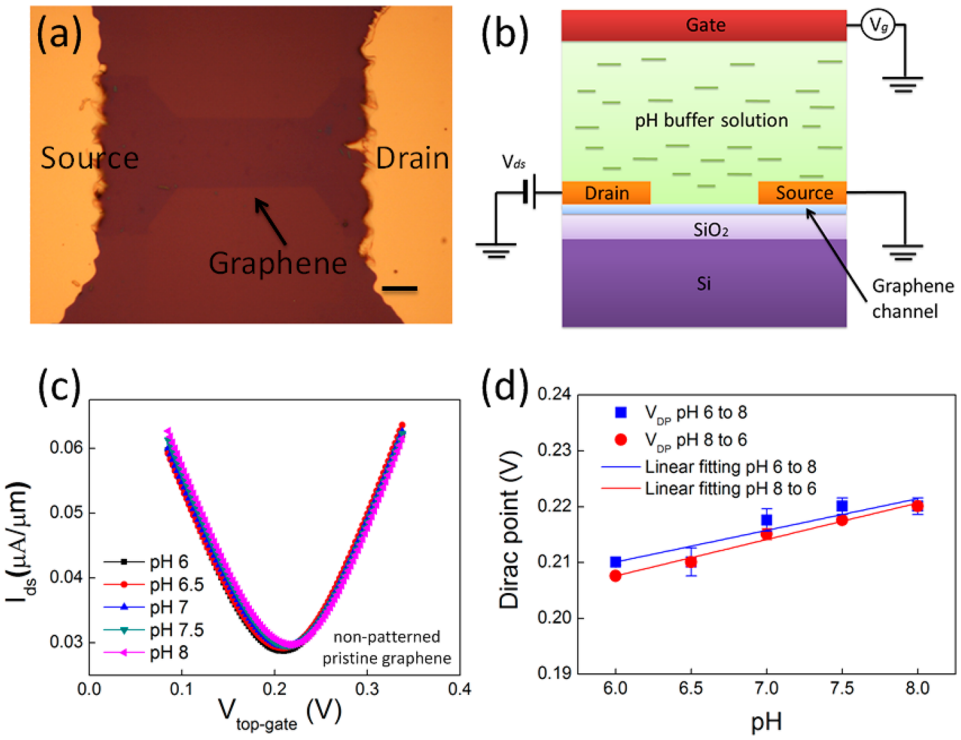

Figure 2. (a) An optical image of graphene FET before edge patterning. The scale bar is 20 μm. (b) Schematic illustration of the working principle of electrolyte-gated graphene FET pH sensor. (c) Measured source-drain current density I_{ds} as a function of the top gate reference potential $V_{top\text{-}gate}$ in different pH buffer solution for nonpatterned pristine graphene FET. (d) The Dirac point shift in response to the different pH. The error bars show the standard deviation of the pH response.

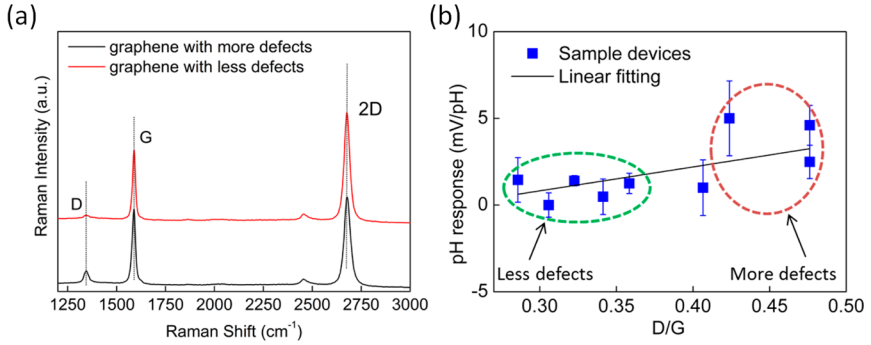

Figure 3. (a) Raman spectrum of the graphene samples with different intrinsic defects. (b) pH response correlated to the Raman peak intensities of G (1588 cm^{-1})/D (1344 cm^{-1}). The error bars show the standard deviation of the pH response.

concentration and temperature. The Dirac point is determined by the applied gate voltage where the electrical conductivity or source-drain current (I_{ds}) is minimum. As the gate voltage is swept from the left side to right side of the Dirac point, the doping in the graphene changes from p-type to n-type. When the pH in the electrolyte is increased, the I_{ds} vs V_g curve and the Dirac point shift toward the positive voltage direction with the increased amount of net p-doping. By measuring the shift of the Dirac point, the change of pH in the electrolyte can be monitored. The sensitivity is defined as the drift of Dirac point voltage (mV) divided by pH change.

Figure 2c shows a typical transfer curve of source-drain current I_{ds} as a function of the applied electrolyte gate voltage measured at a constant drain-source voltage (V_{ds}) of 10 mV, where the drain-source current was normalized to the width of the graphene channel. The V-shaped $I_{ds}-V_g$ curves indicate nearly symmetrical ambipolar behavior. To minimize the hysteretic effect, we took several measurements at each pH to make sure that the random drift of the $I_{ds}-V_g$ curves between different measurements at the same pH was negligibly small. The Dirac point of the device in Figure 2c is around 0.22 V at pH 7, suggesting that the graphene channel is p-doped.[20] When the gate voltage is swept between 0.07 and 0.32 V, the minimum and maximum current densities are determined to be 0.03 and 0.062 μA/μm from pH 6 to 8, respectively. The mobility (μ) of the device is derived from the $I_{ds}-V_g$ curve using the equation $\mu = (1/C_g)(\delta\sigma/\delta V_g)$,[9] where C_g is the quantum capacitance of the graphene (~20 nF cm^{-2}),[28,29] σ is the conductance, and V_g is the gate voltage. The calculated hole and electron mobility are almost the same (1.25×10^3 cm^2 V^{-1} s^{-1}). When the electrolyte pH increases from 6 to 8, the Dirac point shifts slightly from 0.21 to 0.223 V, yielding a low pH response of ~6 mV/pH. This finding is in good agreement with the pH response values reported by other groups, which

dx.doi.org/10.1021/jp409116r | J. Phys. Chem. C XXXX, XXX, XXX−XXX

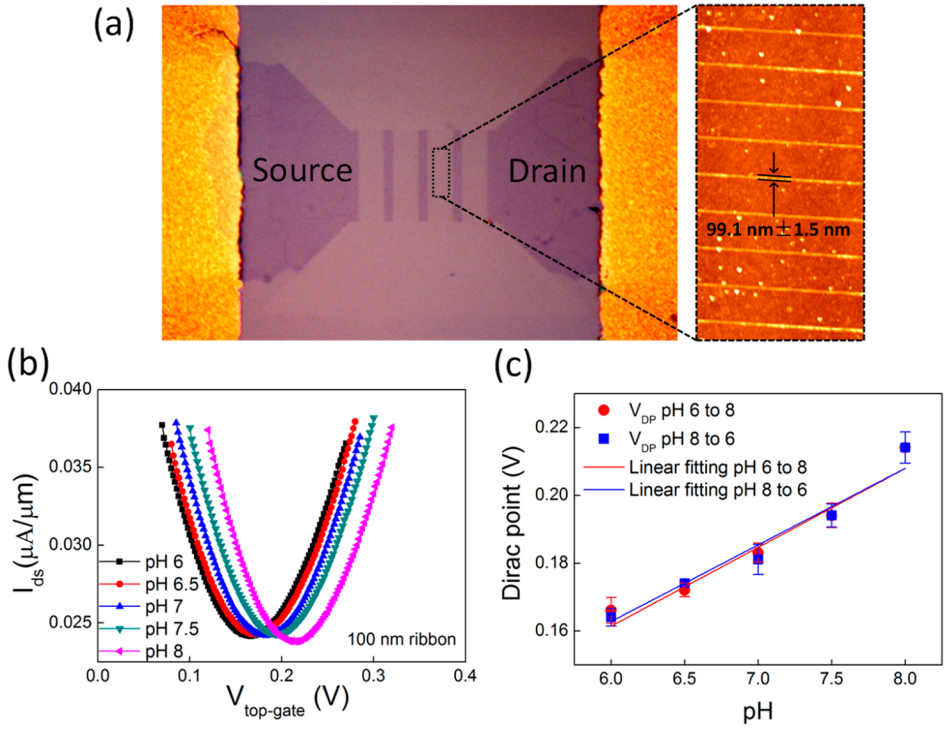

Figure 4. (a) Microscopic image of graphene FET after EBL edge patterning (left); AFM image to show graphene nanoribbons (right). (b) Drain-source current density I_{ds} as a function of the top gate reference potential $V_{top\text{-}gate}$ in different pH buffer solutions for FET made of 100 nm width graphene nanoribbons. (c) Dirac point shift in response to the different pH. The error bars show the standard deviation of the pH response.

indicate that pristine graphene is not sensitive to pH changes.[9,13,14] The weak pH response of our graphene FETs along with their reasonably high mobility demonstrates that our CVD graphene is of high quality.[11] For practical pH sensing applications, the measurement results should not be affected by any historic ions or charge effects. Thus, we measured the Dirac point shift with both increasing pH from 6 to 8 and decreasing pH from 8 to 6. Figure 2d shows that the pH response is 6 mV/pH as the pH increases from 6 to 8 and 6.5 mV/pH as the pH decreases from 8 to 6, indicating that the pH response of our graphene FETs is reversible. The reversibility of the graphene FET devices is consistent with the protonization and deprotonization of OH^- groups attached to graphene.

Since our graphene was grown by CVD, it is likely to contain a small amount of defects in the basal plane. To understand the impact of the defects on pH response, we performed a combined study of pH response and Raman spectroscopy on a number of graphene FETs.[30] Figure 3a shows the Raman spectra of two representative graphene FETs. The peak at 1344 cm^{-1} (D band) is associated with the lattice disorder of graphene while the peak at 1580 cm^{-1} (G band) corresponds to the vibration of sp^2 bond carbon atoms. The ratio of the D band to G band intensities can be used to quantify the level of defects or disorder in the graphene, where a high D/G ratio corresponds to a higher level of defects or disorder. Figure 3b summarizes the pH response of several graphene FET versus the D/G intensity ratio. The pH response increases with the D/G ratio (or defect level in the graphene). The higher pH response in more defective devices can be attributed to the increased number of active dangling bonds on the defect sites that allow adsorption of H_3O^+ or OH^- groups. The sensitivity enhancement can also be affected by the Poole−Frenkel conduction regime where the electrons could hop through the defects.[31]

Encouraged by this interesting finding, we developed a novel approach to improve the pH response of graphene FETs by engineering edge defects. Figure 4a shows the microscopic image of a graphene FET consisting of GNR arrays patterned by EBL and oxygen plasma. The graphene channel consisted of four columns of ribbons connected by large graphene islands, where each GNR was determined to be 99.1 ± 1.5 nm wide, 5.5 μm long, and mostly 1−2 layer by atomic force microscope (AFM). Before testing, the device was annealed at 600 °C with flow of forming gas (H_2/Ar) to remove the resist residue.[27] Figure 4b shows the transfer curve (I_{ds}−V_g) of a FET device consisting of 100 nm wide GNR arrays. Although the total channel width was reduced from 50 to 2 μm after patterning, the current density I_{ds} remains nearly the same. The mobility of GNRs FET also remains essentially the same (1.02×10^3 cm^2 V^{-1} s^{-1}) compared to the pristine graphene FETs, suggesting that introducing edge defects would not degrade the electronic property of the graphene FETs. On the other hand, we observed a significant improvement of pH response increasing from ∼6.5 to ∼23.6 mV/pH by patterning the graphene channel into arrays of narrow GNRs (∼100 nm wide). The strong enhancement of the pH response can be largely attributed to the increase of dangling bonds associated with the increase of total edge length per unit area after patterning the graphene channel into GNRs. Similar effects were observed in gas detection in atmosphere environment using graphene nanoribbons.[22] We also noticed that there was a small systematic shift of the Dirac point toward the negative voltages (0.16 V) in the GNR FET compared to the pristine graphene FET device before patterning (0.21 V). This could be attributed to the remaining resist residue from the fabrication process.[32] To further verify that the enhancement of the pH response in GNR FETs is primarily caused by the creation of more edges rather than by impurities such as resist residue,

dx.doi.org/10.1021/jp409116r | J. Phys. Chem. C XXXX, XXX, XXX−XXX

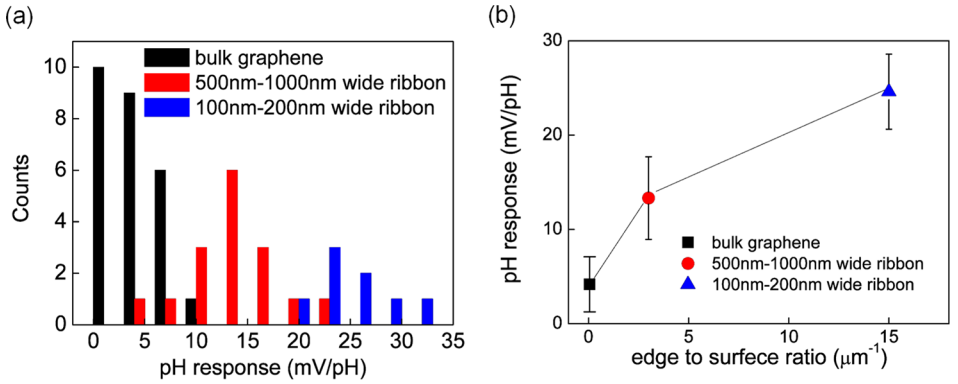

Figure 5. (a) Histogram of sensitivity for the FETs with pristine graphene and graphene ribbons of various widths, pH response of different devices (mV/pH). (b) Average pH response with different edge to surface area ratio. The error bars show the standard deviations.

HSQ resist was also used to pattern GNRs. After development and oxygen plasma etching to form GNRs, HSQ was removed by buffered oxide etch (BOE) to minimize the doping effects.[21,26] Similar pH response values were observed in GNR FETs pattered using HSQ as with PMMA. Figure 4c shows the Dirac point position versus pH for the GNR FET device as the pH changes from pH 6 to 8 and then from pH 8 to 6. The pH response of the patterned GNR device is determined to be 23.6 and 24 mV/pH, respectively. This result demonstrates that the pH response of GNRs is significantly higher than that of large area graphene and the pH response in GNR FETs is also reversible as in large area graphene FETs.

Figure 5 summarizes the results from over 40 devices divided into three categories: pristine graphene, wide GNRs of width 500−1000 nm, and narrow GNR of width 100−200 nm. Figure 5a shows the histogram of the pH response of the devices clearly revealing that the pH response increases with reducing GNR width. The lowest (~0 mV/pH) and highest (30.6 mV/pH) sensitivity values were found in a pristine graphene FET and a 100 nm wide GNR device, respectively. The highest pH response of the pristine graphene FET was about 9.6 mV/pH, and the lowest pH response of 100 nm graphene ribbon was above 20 mV/pH. The average pH response for pristine graphene, 500−1000 nm ribbons, and the 100−200 nm ribbon pattern was determined to be 4.2, 13.5, and 24.6 mV/pH as shown in Figure 5b. Obviously, increasing edge defect sites by reducing the GNR width efficiently improves the pH response.

The sensitivity and sensing mechanisms of graphene-based FET are still under debate. Ohno[14] reported a sensitivity of 50 mV/pH in an electrolyte-gated graphene field-effect transistors (GFET) made of mechanically exfoliated graphene. Cheng[13] reported a sensitivity of 25 mV/pH of a suspended graphene sensor with improved signal-to-noise ratio by removing underneath SiO_2 with HF. Nevertheless, Fu showed that the large variation of the pH response may be associated with the quality of the graphene samples in terms of how they were prepared.[11] Here, we have shown that engineering edge defects significantly improves the pH response of graphene FETs in aqueous solutions. Controllable line edge defects can be created by patterning pristine graphene into graphene nanoribbons using EBL and oxygen plasma. The nanofabrication process does not noticeably degrade the electronic and electrochemical properties of the graphene FETs. The number of edge defect sites for pH sensing can be increased by reducing the width of GNRs, leading to the enhancement of pH response.

CONCLUSIONS

In this paper, we demonstrated that higher pH response of graphene FETs can be achieved by introducing edge defects. The edge defects were created by patterning the graphene into GNR arrays using electron beam lithography and oxygen plasma. We have observed pH response increasing from 4.2 to 24.6 mV/pH when the edge length to surface area ratio increases from 0.04 to 20 μm^{-1}. We also demonstrated that the pH sensing is reversible for both pristine and patterned graphene FET.

AUTHOR INFORMATION

Corresponding Author

*E-mail: mcheng@eng.wayne.edu (M.M.-C.C.).

Notes

The authors declare no competing financial interest.

ACKNOWLEDGMENTS

This work was done in the nFab at Wayne State University and was supported by NSF CAREER Award (1055932) MRI Award (1229635) and Wayne State University. Z. Zhou, H. J. Chuang, and M. W. Lin were supported by NSF-ECCS 1128297. We thank V. Ray for the help of EBL that was performed in part at the Lurie Nanofabrication Facility, a member of the National Nanotechnology Infrastructure Network, which is supported in part by the National Science Foundation.

REFERENCES

(1) Balandin, A. A.; Ghosh, S.; Bao, W.; Calizo, I.; Teweldebrhan, D.; Miao, F.; Lau, C. N. Superior Thermal Conductivity of Single-Layer Graphene. *Nano Lett.* **2008**, *8*, 902−907.

(2) Ghosh, S.; Calizo, I.; Teweldebrhan, D.; Pokatilov, E. P.; Nika, D. L.; Balandin, A. A.; Bao, W.; Miao, F.; Lau, C. N. Extremely High Thermal Conductivity of Graphene: Prospects for Thermal Management Applications in Nanoelectronic Circuits. *Appl. Phys. Lett.* **2008**, *92*, 151911.

(3) Seol, J. H.; Jo, I.; Moore, A. L.; Lindsay, L.; Aitken, Z. H.; Pettes, M. T.; Li, X.; Yao, Z.; Huang, R.; Broido, D.; et al. Two-Dimensional Phonon Transport in Supported Graphene. *Science* **2010**, *328*, 213−216.

(4) Bolotin, K. I.; Sikes, K. J.; Jiang, Z.; Klima, M.; Fudenberg, G.; Hone, J.; Kim, P.; Stormer, H. L. Ultrahigh Electron Mobility in Suspended Graphene. *Solid State Commun.* **2008**, *146*, 351−355.

(5) Ponomarenko, L. A.; Schedin, F.; Katsnelson, M. I.; Yang, R.; Hill, E. W.; Novoselov, K. S.; Geim, A. K. Chaotic Dirac Billiard in Graphene Quantum Dots. *Science* **2008**, *320*, 356−358.

(6) Chen, J.-H.; Jang, C.; Xiao, S.; Ishigami, M.; Fuhrer, M. S. Intrinsic and Extrinsic Performance Limits of Graphene Devices on SiO_2. *Nat. Nanotechnol.* **2008**, *3*, 206−209.
(7) Chen, F.; Xia, J.; Ferry, D. K.; Tao, N. Dielectric Screening Enhanced Performance in Graphene Fet. *Nano Lett.* **2009**, *9*, 2571−2574.
(8) Schedin, F.; Geim, A. K.; Morozov, S. V.; Hill, E. W.; Blake, P.; Katsnelson, M. I.; Novoselov, K. S. Detection of Individual Gas Molecules Adsorbed on Graphene. *Nat. Mater.* **2007**, *6*, 652−655.
(9) Ang, P. K.; Chen, W.; Wee, A. T. S.; Loh, K. P. Solution-Gated Epitaxial Graphene as pH Sensor. *J. Am. Chem. Soc.* **2008**, *130*, 14392−14393.
(10) Shao, Y. Y.; Wang, J.; Wu, H.; Liu, J.; Aksay, I. A.; Lin, Y. H. Graphene Based Electrochemical Sensors and Biosensors: A Review. *Electroanalysis* **2010**, *22*, 1027−1036.
(11) Fu, W. Y.; Nef, C.; Knopfrnacher, O.; Tarasov, A.; Weiss, M.; Calame, M.; Schonenberger, C. Graphene Transistors Are Insensitive to pH Changes in Solution. *Nano Lett.* **2011**, *11*, 3597−3600.
(12) Ristein, J.; Zhang, W. Y.; Speck, F.; Ostler, M.; Ley, L.; Seyller, T. Characteristics of Solution Gated Field Effect Transistors on the Basis of Epitaxial Graphene on Silicon Carbide. *J. Phys. D: Appl. Phys.* **2010**, *43*, 345303.
(13) Cheng, Z. G.; Li, Q.; Li, Z. J.; Zhou, Q. Y.; Fang, Y. Suspended Graphene Sensors with Improved Signal and Reduced Noise. *Nano Lett.* **2010**, *10*, 1864−1868.
(14) Ohno, Y.; Maehashi, K.; Yamashiro, Y.; Matsumoto, K. Electrolyte-Gated Graphene Field-Effect Transistors for Detecting pH Protein Adsorption. *Nano Lett.* **2009**, *9*, 3318−3322.
(15) Heller, I.; Chatoor, S.; Mannik, J.; Zevenbergen, M. A. G.; Dekker, C.; Lemay, S. G. Influence of Electrolyte Composition on Liquid-Gated Carbon Nanotube and Graphene Transistors. *J. Am. Chem. Soc.* **2010**, *132*, 17149−17156.
(16) Larrimore, L.; Nad, S.; Zhou, X. J.; Abruna, H.; McEuen, P. L. Probing Electrostatic Potentials in Solution with Carbon Nanotube Transistors. *Nano Lett.* **2006**, *6*, 1329−1333.
(17) Robinson, J. A.; Snow, E. S.; Badescu, S. C.; Reinecke, T. L.; Perkins, F. K. Role of Defects in Single-Walled Carbon Nanotube Chemical Sensors. *Nano Lett.* **2006**, *6*, 1747−1751.
(18) Zhang, Y. H.; Chen, Y. B.; Zhou, K. G.; Liu, C. H.; Zeng, J.; Zhang, H. L.; Peng, Y. Improving Gas Sensing Properties of Graphene by Introducing Dopants and Defects: A First-Principles Study. *Nanotechnology* **2009**, *20*, 185504.
(19) Ferrari, A. C. Raman Spectroscopy of Graphene and Graphite: Disorder, Electron-Phonon Coupling, Doping and Nonadiabatic Effects. *Solid State Commun.* **2007**, *143*, 47−57.
(20) Wang, X.; Li, X.; Zhang, L.; Yoon, Y.; Weber, P. K.; Wang, H.; Guo, J.; Dai, H. N-Doping of Graphene through Electrothermal Reactions with Ammonia. *Science* **2009**, *324*, 768−771.
(21) Brenner, K.; Yang, Y. X.; Murali, R. Edge Doping of Graphene Sheets. *Carbon* **2012**, *50*, 637−645.
(22) Salehi-Khojin, A.; Estrada, D.; Lin, K. Y.; Bae, M. H.; Xiong, F.; Pop, E.; Masel, R. I. Polycrystalline Graphene Ribbons as Chemiresistors. *Adv. Mater.* **2012**, *24*, 53−57.
(23) Lin, M.-W.; Ling, C.; Agapito, L. A.; Kioussis, N.; Zhang, Y.; Cheng, M. M.-C.; Wang, W. L.; Kaxiras, E.; Zhou, Z. Approaching the Intrinsic Band Gap in Suspended High-Mobility Graphene Nanoribbons. *Phys. Rev. B* **2011**, *84*, 125411.
(24) Li, X. S.; Cai, W. W.; An, J. H.; Kim, S.; Nah, J.; Yang, D. X.; Piner, R.; Velamakanni, A.; Jung, I.; Tutuc, E.; et al. Large-Area Synthesis of High-Quality and Uniform Graphene Films on Copper Foils. *Science* **2009**, *324*, 1312−1314.
(25) Liang, X. L.; Sperling, B. A.; Calizo, I.; Cheng, G. J.; Hacker, C. A.; Zhang, Q.; Obeng, Y.; Yan, K.; Peng, H. L.; Li, Q. L.; et al. Toward Clean and Crackless Transfer of Graphene. *ACS Nano* **2011**, *5*, 9144−9153.
(26) Dan, Y. P.; Lu, Y.; Kybert, N. J.; Luo, Z. T.; Johnson, A. T. C. Intrinsic Response of Graphene Vapor Sensors. *Nano Lett.* **2009**, *9*, 1472−1475.
(27) Wang, X. R.; Tabakman, S. M.; Dai, H. J. Atomic Layer Deposition of Metal Oxides on Pristine and Functionalized Graphene. *J. Am. Chem. Soc.* **2008**, *130*, 8152−8153.
(28) Fang, T.; Konar, A.; Xing, H. L.; Jena, D. Carrier Statistics and Quantum Capacitance of Graphene Sheets and Ribbons. *Appl. Phys. Lett.* **2007**, *91*, 092109.
(29) Guo, J.; Yoon, Y.; Ouyang, Y. Gate Electrostatics and Quantum Capacitance of Graphene Nanoribbons. *Nano Lett.* **2007**, *7*, 1935−1940.
(30) Ferrari, A. C.; Meyer, J. C.; Scardaci, V.; Casiraghi, C.; Lazzeri, M.; Mauri, F.; Piscanec, S.; Jiang, D.; Novoselov, K. S.; Roth, S.; et al. Raman Spectrum of Graphene and Graphene Layers. *Phys. Rev. Lett.* **2006**, *97*, 187401.
(31) Salehi-Khojin, A.; Field, C. R.; Yeom, J.; Masel, R. I. Sensitivity of Nanotube Chemical Sensors at the Onset of Poole-Frenkel Conduction. *Appl. Phys. Lett.* **2010**, *96*, 163110.
(32) Pirkle, A.; Chan, J.; Venugopal, A.; Hinojos, D.; Magnuson, C. W.; McDonnell, S.; Colombo, L.; Vogel, E. M.; Ruoff, R. S.; Wallace, R. M. The Effect of Chemical Residues on the Physical and Electrical Properties of Chemical Vapor Deposited Graphene Transferred to SiO_2. *Appl. Phys. Lett.* **2011**, *99*, 122108.